HEALTH AND MEDICINE

Low-intensity pulsed ultrasound elevates blood pressure for shock

Chenrui Wu[1]†, Yu Tian[1]†, Tao Liu[1]†‡, Shuo An[1], Yu Qian[1], Chuang Gao[1], Jiangyuan Yuan[1], Mingqi Liu[1]§, Meng Nie[1], Weiwei Jiang[1]¶, Zhuang Sha[1], Chuanxiang Lv[1], Qiang Liu[2], Xiaochun Wang[3]*, Sheng Zhou[3]*, Rongcai Jiang[1]*‡

Fluid replacement is the primary treatment for life-threatening shock but is challenging in harsh environments. This study explores low-intensity pulsed ultrasound (LIPUS) as a resuscitation strategy. Cervical LIPUS stimulation effectively elevated blood pressure in shocked rats. It also improved cerebral and multiorgan perfusion. Mechanistically, LIPUS activated pathways related to sympathetic nerve excitation and vascular smooth muscle contraction, increasing plasma catecholamines and stimulating blood pressure–regulating neural nuclei. Partial sympathetic nerve transection reduced LIPUS efficacy, while complete inhibition of these nuclei abolished the response. Preliminary clinical trials demonstrated LIPUS's ability to raise blood pressure in shock patients. The findings suggest that LIPUS enhances sympathetic nerve activity and activates blood pressure–regulating nuclei, offering a noninvasive, neuromodulation-based approach to shock treatment. This method holds potential for improving blood pressure and organ perfusion in shock patients, especially in resource-limited environments.

INTRODUCTION

Shock is a critical medical condition characterized by inadequate blood flow to the body's tissues, resulting in cellular dysfunction and organ failure. Hemorrhagic shock, a type of common shock, provoked by severe loss of blood causing insufficient tissue perfusion and cellular oxygen deficit, is a notable contributor to morbidity and mortality globally (*1*). Common causes encompass traumatic injury, severe burns, major surgeries, childbirth, gastrointestinal bleeding, or other severe bleeding episodes such as from ruptured blood vessels or aneurysms (*2*). Mortality rates can be as high as 60% in severe cases of hemorrhagic shock (*3*). Septic and cardiogenic shocks are prevalent forms of shock. In the United States, approximately 2% of hospital admissions are for septic shock, with mortality rates approaching 20 to 30% (*4*). Annually, cardiogenic shock affects 40,000 to 50,000 Americans and carries a mortality rate of about 50% (*5*, *6*). Despite the type, the fundamental manifestation of shock is the difficulty in maintaining adequate circulation, leading to insufficient oxygen and nutrient delivery to tissues, which is essential for cellular and organ function. This consequence makes immediate and effective management critical to avoid progressing down the path of multi-organ dysfunction syndrome (MODS) and death (*7*). The primary therapeutic measures for shock involve hemodynamic stabilization and restoration of adequate organ perfusion.

Initial remedial processes for hemorrhagic shock have made a revolutionary shift over the years, predominantly focusing on hemorrhage control, volume replacement by fluid resuscitation, and correction of coagulopathy. Notwithstanding, the mortality rates remain high due to the persistent risk of entering an irreversible stage of shock (*8*). Resuscitation strategies conventionally resort to substantial intravenous fluids for restoration of lost blood volume (*9*). However, the risk-to-benefit ratio of this approach remains controversial, considering its potential downside to incite dilution of clotting factors, hypothermia, and consequent hyperinflammatory state (*10*, *11*). Furthermore, in settings like factories, underdeveloped regions, and battlefields, the availability of intravenous fluid resuscitation therapy is often limited by the absence of both medical professionals and available facilities, leading to higher mortality rates from shock. The development of straightforward and feasible methods to elevate blood pressure (BP) could enhance access to treatment and potentially decrease shock-related mortality.

Given that circulatory failure is a central characteristic of all types of shock, elevating BP remains a critical component in their treatment. However, traditional reliance on infusion to raise BP presents challenges in implementation, while the use of hemodynamic drugs to increase BP can lead to peripheral organ ischemia and is not sustainable. Given these challenges, we have focused on neuromodulation as a method to elevate BP (*12*) following shock. An emerging, potential game-changer is the use of low-intensity pulsed ultrasound (LIPUS), a clinically noninvasive method. LIPUS's ability to cause mechanical effects presents a promising therapeutic tool for a number of medical conditions, including neurological disorders, tumors, and targeted drug delivery (*13*). LIPUS essentially uses acoustic energy at lower intensities and frequencies, providing a noninvasive and effective method of tissue stimulation and manipulation (*14*). Thus, LIPUS can be used as a noninvasive neuromodulatory tool that can have a variety of effects, including BP regulation, depending on the target site. In neuroscience, the application of LIPUS has gained considerable attention, chiefly for its ability to target deeper regions of the brain while maintaining a noninvasive approach. This trait of neuromodulation, manipulating

[1]Department of Neurosurgery, Tianjin Neurological Institute, State Key Laboratory of Experimental Hematology, Key Laboratory of Post-Neuroinjury Neurorepair and Regeneration in Central Nervous System Tianjin & Ministry of Education, Tianjin Medical University General Hospital, Tianjin 300052, China. [2]Department of Neurology, Institute of Neuroimmunology, Tianjin Medical University General Hospital, Tianjin 300052, China. [3]Institute of Biomedical Engineering, Chinese Academy of Medical Sciences and Peking Union Medical College, Tianjin 300052, China.
*Corresponding author. Email: tjwxc@126.com (X.W.); zhousheng@bme.pumc.edu.cn (S.Z.); jiangrongcai@tmu.edu.cn (R.J.)
†These authors contributed equally to this work.
‡Present address: Department of Neurosurgery, Xuanwu Hospital, Capital Medical University, Beijing 100053, China.
§Present address: Department of Rehabilitation Medicine, Zhejiang Provincial People's Hospital, Hangzhou, Zhejiang Province 310014, China.
¶Present address: Department of Rehabilitation Medicine, Zhujiang Hospital, Southern Medical University, Guangzhou 510282, China.

nerve activity by delivering a specifically aimed stimulation, offers a groundbreaking means of treating neurological or psychiatric conditions (*15*). The application of 0.5 to 5 min of ultrasound stimulation has been demonstrated to yield enduring neuroregulatory effects, persisting from several minutes to several hours (*16*). Clinical research spearheaded by Martínez-Fernández *et al.* (*17*, *18*) demonstrated the successful implementation of focused ultrasound in managing tremors associated with Parkinson's disease, recording appreciable reductions in motor disability scores. Furthermore, in the scope of Alzheimer's disease, promising advancements have been uncovered with LIPUS; preclinical trials revealed that repeated ultrasound sessions fostered clearance of β-amyloid plaques, consequently enhancing cognitive functions (*19*). Beyond neurodegenerative disease, prolonged ultrasound stimulation has been noted to elicit excitation-like effects and induce alterations in connectivity in both nonhuman primates (NHPs) and human subjects, with effects lasting for over an hour. Specifically, stimulation of the amygdala and supplementary motor area in NHPs has been shown to influence circuit connectivity, leading to a modification in the coupling of functional magnetic resonance imaging (fMRI)–observed activity between the focused ultrasound targets and other brain regions (*20*, *21*). The efficacy of LIPUS is contingent upon the stimulation target, with targeted stimulation of the autonomic nervous system serving as the theoretical foundation for its regulation of vital signs, including BP.

LIPUS has been proven to be effective in neuromodulation, but there have been no studies for increasing BP. Hypotension is a hallmark of shock, and our pioneering study investigated the effects and mechanisms of noninvasive cervical LIPUS stimulation on BP regulation in rats with hemorrhagic shock. Additionally, we executed a small-scale, self-controlled, before-and-after clinical trial to evaluate the clinical translatability of LIPUS.

RESULTS

LIPUS stimulation increased the BP of rats

Here, we confirmed the effect of LIPUS stimulation on increasing BP in normal and hemorrhagic shock rats through arterial monitoring, plasma metabolomics, blood oxygenation level–dependent fMRI (BOLD-fMRI), etc., and explored the mechanisms of LIPUS stimulation elevating BP (Fig. 1A). A minimum of 5 min of BP monitoring was performed on rats before cervical LIPUS stimulation, followed by 10 min of stimulation, and 5 min of continued monitoring after stopping the stimulation (Fig. 1B).

The BP of the rats varied to different extents after stimulation at 1, 2, and 3 W/cm^2 spatial peak pulse average intensity (Isppa) (Fig. 2, A to C). We found that at 1 W/cm^2, the BP and heart rate (HR) of the rat had no noticeable change (1 W/cm^2: $P > 0.05$, pre versus LIPUS; Fig. 2D), whereas after stimulation at 2 and 3 W/cm^2 Isppa, there was a noticeable rise in the rat's BP (2 to 3 W/cm^2: $P < 0.001$, pre versus LIPUS; Fig. 2, E and F); the HR of the rat also rose after stimulation at 3 W/cm^2 Isppa (3 W/cm^2: $P < 0.05$, pre versus LIPUS; Fig. 2F). At the same time, after stopping the stimulation, the rat's BP would gradually drop back to prestimulation levels (2 to 3 W/cm^2: $P < 0.01$, LIPUS versus post; Fig. 2, E and F). On the basis of the above results, 2 W/cm^2 Isppa can effectively increase the rat's BP and have no noticeable effect on the HR, and we chose this intensity for cervical stimulation in subsequent experiments. To exclude the influences of skin temperature rise and pain caused by ultrasound thermal effects and mechanical effects on the rat's BP and HR, we

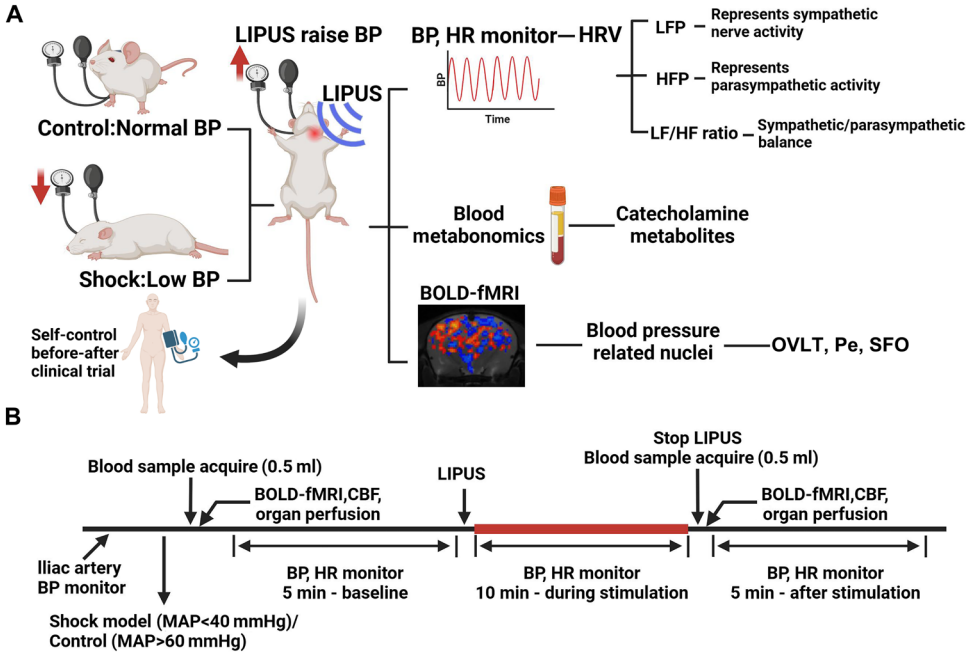

Fig. 1. The schematic of the study. (**A**) A diagram shows the elevation of BP through cervical LIPUS stimulation in both normotensive rats and rats with shock-induced BP. The study also explores the effects and potential mechanisms of LIPUS in raising BP through arterial monitoring, HRV analysis, plasma metabolomics analysis, and BOLD-fMRI. A small-scale self-control before-after clinical trial was performed to explore the clinical translational potential of LIPUS. (**B**) The timeline outlines the design and progression of animal experiments in the study.

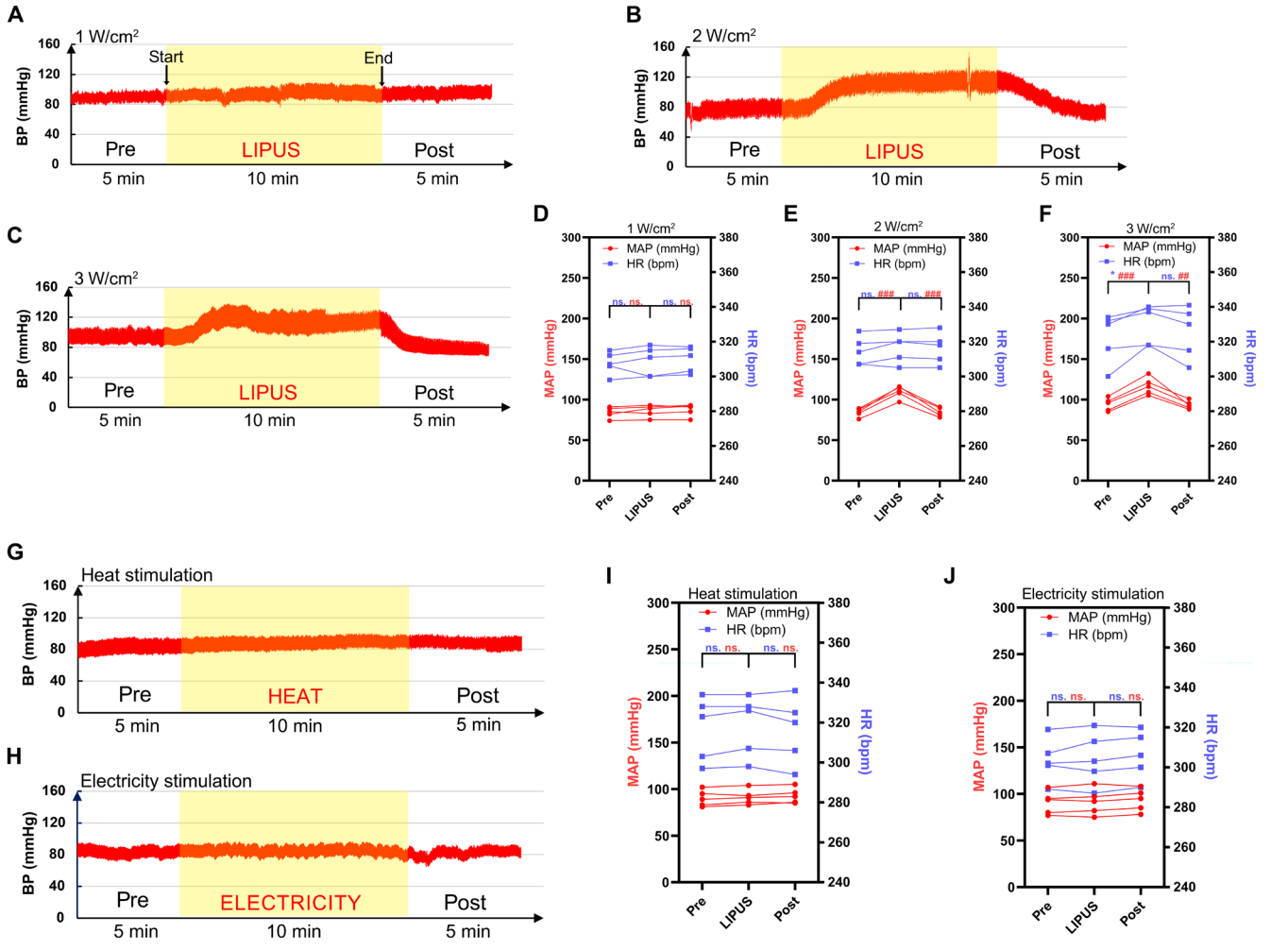

Fig. 2. Cervical LIPUS stimulation elevated BP in rats. (**A** to **C**) BP monitoring data in Sprague-Dawley rats after cervical LIPUS stimulation with different spatial peak pulse average intensity (Isppa) of 1, 2, and 3 W/cm^2. (**D** to **F**) Effect of cervical LIPUS stimulation with different effective ultrasound intensities on BP and HR in Sprague-Dawley rats ($n = 5$; ns., not significant; HR: $^{*}P < 0.05$; MAP: $^{\#\#}P < 0.01$, $^{\#\#\#}P < 0.001$). (**G** and **H**) Arterial BP monitoring data after cervical skin electrical stimulation and cervical skin thermal stimulation. (**I** and **J**) Statistical analysis of MAP and HR data after cervical skin electrical stimulation and cervical skin thermal stimulation ($n = 5$).

performed a continuous 10-min 3-mA 10-Hz electrical stimulation (Fig. 2G) and a 40°C heat stimulation (Fig. 2H) on the rat's cervical skin. The monitoring data of BP and HR show that neither skin electrical stimulation nor heat stimulation had noticeable effects on the rat's BP and HR ($P > 0.05$, pre versus LIPUS; Fig. 2, I and J). The above results indicate that cervical LIPUS stimulation can effectively increase the BP of rats, and it is not related to the thermal effects or pain stimulation of ultrasound. To further explore the potential physiological mechanisms of cervical LIPUS stimulation in increasing BP, we studied the cervical sympathetic nerve (SN) trunk or vagus nerve (VN). After the transection of the SN or the VN on the same side of the stimulation, we monitored the reactivity of rat BP to LIPUS stimulation (fig. S1, A and B). We found that after the cervical SN or the VN was severed, the BP still increased after the stimulation (fig. S1, A and B), but after cervical SN transection, the extent of BP rise [ΔMAP (mean arterial pressure) = average MAP during LIPUS − average MAP before LIPUS] was significantly reduced ($^{**}P < 0.01$, SN transection versus control; fig. S1C), whereas after VN transection, there was no noticeable change in the extent of the BP rise ($P > 0.05$, VN transection versus control; fig. S1C). After severing SN, the increase in BP is diminished, suggesting that the mechanism by which LIPUS stimulation elevates BP is linked to SN excitation.

LIPUS stimulation increases the BP of hemorrhagic shock rats

We confirmed the effect of cervical LIPUS stimulation in increasing BP in normal rats. Furthermore, we explored whether LIPUS has a similar BP-elevating effect for shock in the shock rat model. We established the hemorrhagic shock model in rats by placing the tube in the rat's femoral artery to monitor their BP, and simultaneously bleeding them until their MAP was less than 40 mmHg. Consistent with the timeline of previous experiments, rats were monitored for at least 5 min of baseline BP before 10 min of cervical LIPUS stimulation, and monitoring was continued for 5 min after the stimulation (Fig. 3A). Under the stimulation of 2 W/cm^2 Isppa, the BP of normal rats raised ($P < 0.0001$, pre versus LIPUS; Fig. 3B), accompanied by a slight elevation in HR ($P < 0.05$, pre versus LIPUS;

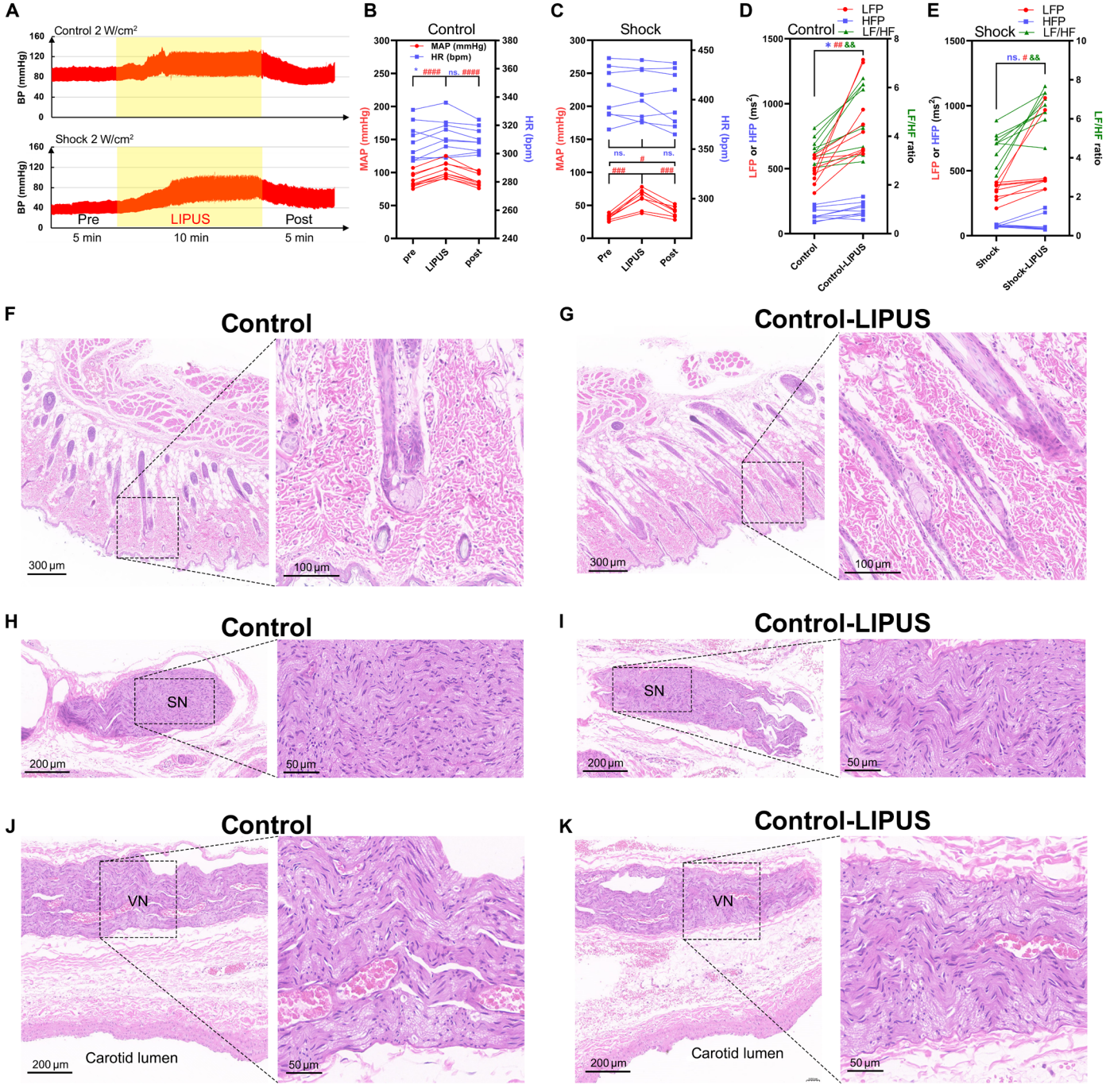

Fig. 3. Cervical LIPUS stimulation increased BP in hemorrhagic shock rats. (**A**) Representative BP monitoring data after stimulation in normal BP and hemorrhagic shock Sprague-Dawley rats. (**B** and **C**) Normal BP group ($n = 9$) and shock group ($n = 8$) statistical analysis of MAP and HR data ($^{*}P < 0.05$; $^{\#}P < 0.05$, $^{\#\#\#}P < 0.001$). (**D** and **E**) Normal BP group ($n = 9$) and shock group ($n = 8$) HRV in the sympathetic/parasympathetic activity–related HFP, LFP, and LF/HF ratio statistical analysis. (**F** and **G**) Representative H&E-stained images of the cervical skin showed that LIPUS stimulation did not affect the superficial skin. (**H** and **I**) Representative H&E staining of SNs showed that LIPUS had no damage to the SNs. (**J** and **K**) Representative sections of the VN and the accompanying carotid artery (carotid lumen) stained with H&E suggest that LIPUS stimulation causes no damage to the VN.

Fig. 3B). After stopping the stimulation in the normal BP group, the BP gradually dropped and returned to the baseline level before the stimulation ($P < 0.0001$, LIPUS versus post; Fig. 3B). At the same time, arterial BP monitoring of hemorrhagic shock rats showed that the baseline MAP was less than 40 mmHg. However, after stimulation, the BP increased significantly ($P < 0.001$, pre versus LIPUS; Fig. 3C), while the HR did not change noticeably ($P > 0.05$, pre versus LIPUS; Fig. 3C). The shock group maintained elevated BP compared to baseline for 5 min following the cessation of stimulation ($P < 0.05$, pre versus post; Fig. 3C). After analysis of the HR variability (HRV) obtained based on the R-R interval data of the electrocardiogram, we obtained the HRV data before and after

cervical LIPUS stimulation of normal BP and shock rats, including low-frequency power (LFP) related to SN excitability, high-frequency power (HFP) related to parasympathetic nerve excitability, and LF/HF ratio related to the balance of sympathetic and parasympathetic nerves. The results show that after cervical LIPUS stimulation, LFP, HFP, and LF/HF of rats in the normal BP group raise to varying degrees (LFP: $P < 0.01$, HFP: $P < 0.05$, LF/HF: $P < 0.01$; Fig. 3D). At the same time, in shock rats, LFP and LF/HF increase significantly after stimulation, and HFP does not change noticeably (LFP: $P < 0.05$, HFP: $P > 0.05$, LF/HF: $P < 0.01$; Fig. 3E).

Safety is a basic premise of a treatment method. To clarify the effect of cervical LIPUS stimulation on superficial and deep tissues, we sliced the superficial skin of the neck, the deep SN trunk, and the VN on the stimulation side and used hematoxylin and eosin (H&E) staining. The results showed that the histological characteristics of the cervical superficial skin tissue without stimulation and after 60 min of stimulation (Fig. 3, F and G), and the deep SNs (Fig. 3, H and I) and VNs (Fig. 3, J and K) were similar, suggesting that there was no noticeable damage after stimulation. Furthermore, Prussian blue staining was performed on cervical tissues. The results showed that no notable microbleeding was observed in the skin, SN, or VN after 60 min of LIPUS stimulation (fig. S2). We first evaluated the effect of cervical LIPUS stimulation in increasing the BP of shock rats and found that the intensity can not only increase BP but also improve cerebral perfusion aftershocks, and the safety is secure.

LIPUS stimulation improves cardiac function and multi-organ perfusion of hemorrhagic shock rats

The low perfusion of organs after hemorrhagic shock is an important cause of poor prognosis. Therefore, it is very important to clarify whether LIPUS stimulation improves the function of the heart and the perfusion of important organs in rats while raising BP. We detected the heart function and blood flow of the liver and kidney in rats by ultrasound, and the perfusion of the cerebral cortex by laser speckle contrast analysis (LASCA). The heart function results showed that the left ventricular ejection fraction (EF) and cardiac output (CO) of the shocked rats were significantly reduced compared to the normal group (EF: $P < 0.05$; CO: $P < 0.0001$; Table 1, Fig. 4A, and fig. S3A). However, LIPUS significantly increased the CO of shocked rats ($P < 0.05$; Table 1 and Fig. 4A), but did not significantly improve the EF ($P = 0.0693$; Table 1 and Fig. 4A). For the kidneys, the peak systolic velocities (PSVs) and end-diastolic velocities (EDVs) of the renal artery and interlobar artery were significantly reduced after shock compared to the normal group (renal artery PSV and EDV: $P < 0.0001$; renal interlobar PSV and EDV: $P < 0.0001$; Table 1, Fig. 4B, and fig. S3B), and the renal artery resistance index (RI) significantly increased (RI: $P < 0.05$; Table 1 and Fig. 4B), indicating that the renal artery resistance increased and kidney perfusion decreased after the shock. While LIPUS increased the PSV and EDV of the renal artery (renal artery PSV and EDV: $P < 0.05$; Table 1 and Fig. 4B), there was no significant improvement in renal artery RI and interlobular PSV and EDV ($P > 0.05$; Table 1 and Fig. 4B). Similar to the kidney, the PSV and EDV of the hepatic artery dropped sharply after shock (hepatic artery PSV and EDV: $P < 0.05$; Table 1 and fig. S3C). Although LIPUS stimulation increased the mean value of hepatic artery PSV and EDV after shock, there was no statistical difference ($P > 0.05$; Table 1). Furthermore, we noninvasively measured the perfusion of the liver and kidneys using arterial spin labeling perfusion MRI (ASL-MRI) (fig. S4, A and B). The ASL-MRI results showed that LIPUS increased the renal cortical perfusion in both the control group and the shock group, with a more pronounced effect in the shock group ($P < 0.05$; fig. S4C). LIPUS also enhanced liver perfusion in the shock group ($P < 0.05$; fig. S4D) but had no significant effect on liver perfusion in the control group ($P > 0.05$; fig. S4D).

To further explore whether stimulation can improve the decline in cerebral perfusion aftershocks, we detected the perfusion of the cerebral cortex through laser speckle (Fig. 4C). Under normal BP conditions, the blood flow of the same side of the brain cortex increases after stimulation ($P < 0.01$; Fig. 4D), and there is no noticeable change on the opposite side ($P > 0.05$; Fig. 4D), whereas under shock conditions, the stimulation can significantly suggest that the cerebral cortex blood flow on both the stimulation side and the opposite side is stimulating ($P < 0.01$; Fig. 4E).

Table 1. Effects of LIPUS stimulation on cardiac function and blood flow of liver and kidney. EDV, end-diastolic velocity; PSV, peak systolic velocity; RI, resistance index; C, control group; S, shock group; S + L = shock + LIPUS group.

	Control ($n = 6$)	Shock ($n = 6$)	Shock + LIPUS ($n = 6$)	*P* value (C vs. S)	*P* value (S vs. S + L)
Ejection fractions (%)	84.1 ± 6.3	71.8 ± 9.2	82.0 ± 6.0	0.0266	0.0693
Cardiac output (ml/min)	90.1 ± 16.2	44.0 ± 9.9	62.8 ± 8.7	<0.0001	0.0409
Renal artery EDV (mm/s)	195.6 ± 50.0	70.6 ± 22.4	135.7 ± 37.7	<0.0001	0.0261
Renal artery PSV (mm/s)	491.2 ± 98.5	260.2 ± 44.3	386.2 ± 48.3	<0.0001	0.0156
Renal artery RI	0.601 ± 0.059	0.731 ± 0.060	0.650 ± 0.081	0.0114	0.1285
Renal interlobar artery EDV (mm/s)	121.8 ± 26.6	58.9 ± 17.1	97.5 ± 33.4	0.0025	0.0579
Renal interlobar artery PSV (mm/s)	285.7 ± 51.9	148.6 ± 37.1	210.0 ± 50.4	0.0004	0.0919
Renal interlobar artery RI	0.576 ± 0.037	0.603 ± 0.078	0.542 ± 0.102	0.8226	0.3850
Hepatic artery EDV (mm/s)	105.6 ± 49.4	23.0 ± 7.4	44.8 ± 10.8	0.0006	0.4275
Hepatic artery PSV (mm/s)	252.4 ± 104.6	96.8 ± 54.0	157.8 ± 103.7	0.0241	0.4900
Hepatic artery RI	0.585 ± 0.072	0.733 ± 0.086	0.628 ± 0.176	0.1174	0.3125

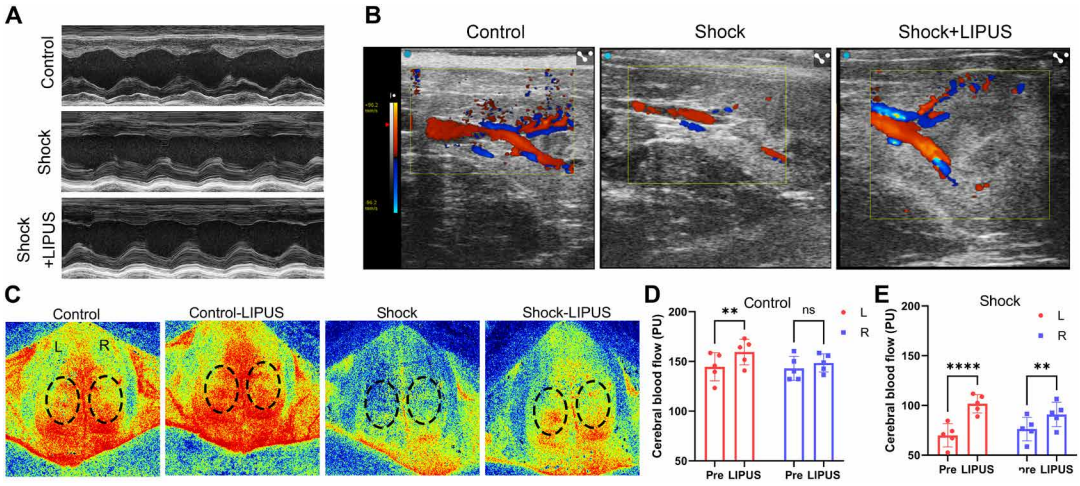

Fig. 4. Cervical LIPUS stimulation improved multiple organ perfusion in hemorrhagic shock rats. (**A**) Representative cross-sectional echocardiography of control, shock, and shock + LIPUS group. (**B**) Representative color Doppler flow images of the renal artery and renal interlobar artery. (**C**) Representative cortical CBF images before and after the stimulation in the normal BP group and shock group were detected by laser speckle contrast imaging instrument. (**D** and **E**) Comparative analysis of the brain perfusion in the bilateral cortex ROIs of the normal BP group and the shock group.

LIPUS stimulation excites SNs, leading to vascular smooth muscle contraction and increased BP

To explore the mechanism of cervical LIPUS stimulation leading to an increase in BP, we performed the metabolomic analysis of plasma in control and shock rats after stimulation or no stimulation (control group, control + LIPUS group, shock group, shock + LIPUS group). The relationship model between each sample established by orthogonal partial least squares discriminant analysis (OPLS-DA) shows that there is a certain difference with good distinguishability between different groups (Fig. 5A). The cyclic heatmap shows the 300 metabolites with the most significant differences in relative expression between each group, suggesting a difference in metabolites between each group (Fig. 5B). Furthermore, the complex heatmap shows the multiple dimension properties of the top 50 most noticeably different metabolites between the four groups, including the ontology, the expression heatmap of each sample, the average expression heatmap of each group, the *P* value, and the VIP (variable importance on projection) value of each sample (Fig. 5C). Why can LIPUS stimulate an increase in BP? This is the focus of our investigation. Therefore, we further analyzed the different metabolites of the shock group and the shock + LIPUS group. The volcano chart shows 133 different metabolite products of the shock group and the shock + LIPUS group (fold change $\geq$ 1.5 or fold change $\leq$ 1/1.5, $P < 0.05$; Fig. 5D). Figure 5E shows the top 30 different metabolites and their fold change and VIP values, such as phosphatidylcholine (PC) (18:0/18:2), 5.6-dihydroxy-2-methylaminotetralin, sphingomyelin (SM) (d18:1/24:1), bauerine C, and PC (20:5/16:0). After performing pathway enrichment analysis on the 133 different metabolites, we found that many pathways related to BP rise were activated, such as vascular smooth muscle contraction, renin secretion, and cyclic guanosine monophosphate-protein kinase G (cGMP-PKG) signaling pathway (Fig. 5F). The results of plasma metabolomics analysis suggest that the potential mechanism for the rise in BP induced by cervical LIPUS stimulation may be the activation of signal pathways related to vascular smooth muscle contraction.

The level of plasma catecholamines increased after LIPUS stimulation and was positively related to SN excitation

We obtained the level of catecholamine metabolites in the shock group and the shock + LIPUS group from the plasma metabolomics data, where epinephrine 3-sulfate and dopamine increased significantly after stimulation ($P < 0.05$; Fig. 6A), while epinephrine and arachidonoyl dopamine did not change noticeably ($P > 0.05$; Fig. 6A). To further determine the relevance of plasma catecholamine levels and HRV indicators related to sympathetic or vagal nerves, we analyzed the relevance of five variables—epinephrine 3-sulfate, dopamine, LFP, HFP, and LF/HF ratio—in each animal in the shock group and the shock + LIPUS group. The results hint that epinephrine 3-sulfate and dopamine have significant positive correlations with the LF/HF ratio (red, $P < 0.0001$; Fig. 6B), while HFP has a negative correlation with epinephrine 3-sulfate, dopamine, and LF/HF ratio, but there is no statistical difference (blue, $P > 0.05$; Fig. 6B). The analysis of plasma catecholamine level and its correlation with HRV suggest that after cervical LIPUS stimulation, SN excitation is closely related to the increase in catecholamine secretion.

LIPUS stimulation activates hypothalamic nuclei associated with BP regulation

BOLD-fMRI results suggest that LIPUS significantly alters the pattern of brain activity in rats, with notable increases in hypothalamic activity (Fig. 6C and fig. S5). Using the rat brain atlas, we extracted and analyzed fractional amplitude of low-frequency fluctuation (fALFF) data from regions associated with BP regulation in the hypothalamus, the organum vascularis of the lamina terminalis (OVLT), the paraventricular nucleus of the hypothalamus (Pe), and the subfornical organ (SFO), designated as regions of interest (ROIs). Statistical outcomes revealed that LIPUS significantly activated OVLT and SFO ($n = 5$; $P < 0.05$; Fig. 6, D and F), while there was an increase in Pe activity, although it did not reach statistical significance ($n = 5$; $P = 0.1019$; Fig. 6E). To further investigate the role of the sympathetic nervous system and specific nuclei in LIPUS-induced BP elevation, we conducted experiments involving

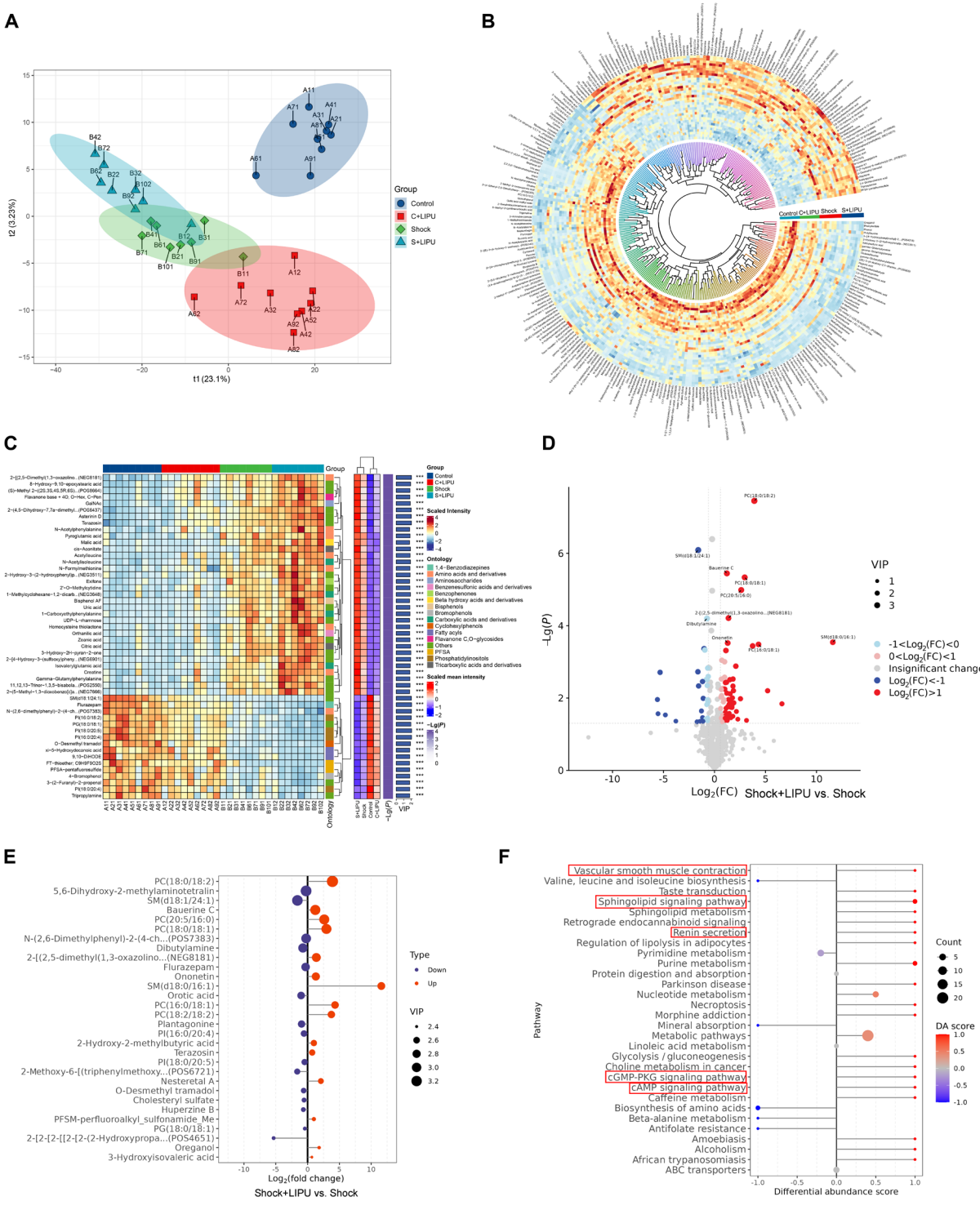

Fig. 5. Plasma metabolomics suggested differentially expressed metabolites and related signaling pathways after cervical LIPUS stimulation. (**A**) OPLS-DA analysis showed the intergroup differences and intra-group variations of samples in the control group ($n = 9$), control + LIPUS group ($n = 9$), shock group ($n = 8$), and shock + LIPUS group ($n = 8$). (**B**) Ring heatmap showing the top 300 significant different metabolites between the control group, control + LIPUS group, shock group, and shock + LIPUS group. (**C**) The complex heatmap displays information on the relative expression levels of the top 50 significantly different metabolites among the control group ($n = 9$), control + LIPUS group ($n = 9$), shock group ($n = 8$), and shock + LIPUS group ($n = 8$). The heatmap includes relative expression values, mean relative values, *P* values, VIP values, and ontology classification information of the metabolites. (**D**) Volcano plot showing the differentially expressed metabolites in plasma before and after LIPUS stimulation in the shock group. (**E**) Top 30 metabolites with VIP values and their fold change in plasma before and after LIPUS stimulation in the shock group. (**F**) The functional clustering diagram of differential metabolites displays the top 30 pathways based on differential abundance (DA) scores (shock + LIPUS versus shock).

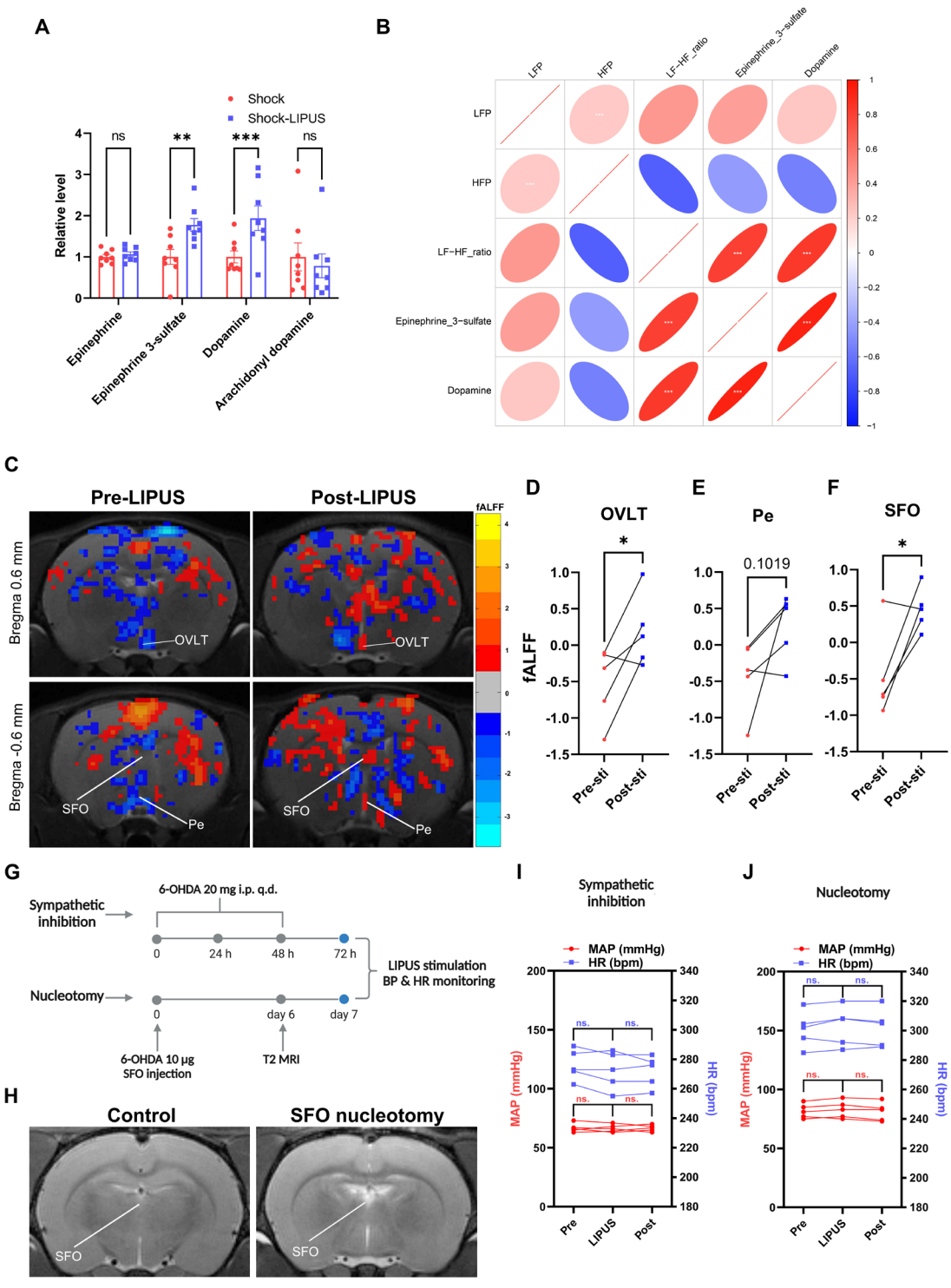

Fig. 6. The level of catecholamine metabolites detected by plasma metabolomics after the shock rat received cervical LIPUS stimulation is related to the excitement of the SN. (**A**) Catecholamine metabolites detected in plasma ($n = 8$; $P < 0.01$, $P < 0.001$; shock-LIPUS versus shock). (**B**) Correlation matrix of LFP, HFP, and LF/HF ratio (HRV), and the plasma epinephrine 3-sulfate and dopamine (catecholamine metabolites) of shock Sprague-Dawley rats ($n = 8$; $^{**}P < 0.001$). (**C**) Representative BOLD-fMRI images indicate that LIPUS activates the hypothalamic nucleus associated with BP regulation, including OVLT, Pe, and SFO. (**D** to **F**) Paired *t* test statistical analysis of fALFF data from the three ROIs (OVLT, Pe, and SFO) before and after LIPUS stimulation ($n = 5$, $^{*}P < 0.05$). (**G**) Flowchart of the sympathetic inhibition and SFO nucleotomy. (**H**) Representative T2WI images suggest that 6-OHDA injection successfully disrupted the SFO nuclei. (**I** and **J**) Cervical LIPUS stimulation had no significant effect on MAP or HR after inhibition of the SNs or SFO nucleotomy ($n = 5$).

SN inhibition and nucleotomy (Fig. 6G). Using T2 weighted imaging (T2WI), we confirmed the destruction of the SFO nucleus in rats, followed by LIPUS stimulation experiments (Fig. 6H). Administration of 6-hydroxydopamine (6-OHDA) effectively inhibited SN activity, completely nullifying the LIPUS effect on BP elevation ($n = 5$; $P > 0.05$; Fig. 6I). Similarly, following SFO nucleotomy, while LIPUS stimulation induced a slight increase in BP, the change was not statistically significant ($n = 5$; $P > 0.05$; Fig. 6J). The fMRI results further reveal the neuromodulation mechanisms of LIPUS stimulation, suggesting that the elevation of BP is associated with the activation of nuclei related to BP regulation. The influence of LIPUS on BP elevation was negated following SN inhibition and SFO nucleotomy. This indicates that the mechanism behind LIPUS-induced BP elevation involves the excitation of the sympathetic nervous system and the activation of BP-associated nuclei, such as the SFO.

Clinical self-control before-after trial suggested that LIPUS stimulation could effectively increase human BP

We conducted a small-scale trial of cervical LIPUS stimulation in 12 shock patients at Tianjin Medical University General Hospital (table S1). The trial was approved by the hospital ethics committee (IRB2023-YX-267-01), and the written consent of the patient or his/her agent was obtained. All patients' BP was obtained by an arterial monitoring device. We applied cervical LIPUS stimulation to shock patients for 5 min and recorded arterial BP data (Fig. 7A). The self-control before-after trial showed that LIPUS elevated systolic BP but had no significant effect on diastolic BP in the shock patients (Fig. 7B).

In conscious healthy volunteers, after 5 min of cervical LIPUS stimulation, the results suggested that the pre- and poststimulation BP and HR of all volunteers were not significantly different from the prestimulation period, and no discomfort was reported (table S2). Elevated BP was not observed in healthy volunteers following LIPUS application, likely due to the limitations of the noninvasive arm cuff. The arm cuff, as an indirect means of measuring BP, does not permit continuous, real-time, and accurate monitoring. Nevertheless, the volunteers did not report any discomfort initially, validating the safety of cervical LIPUS stimulation. The results indicated that cervical LIPUS stimulation can safely increase BP in shock patients, suggesting that LIPUS may be beneficial not only for hemorrhagic shock but also for other types of shock.

DISCUSSION

Here, we observed that LIPUS stimulation of the carotid triangle area improves BP in shock rats. BP is one of the main parameters of hemodynamics, and our discovery is that noninvasive cervical LIPUS stimulation can raise BP, leading to improvement of multiple organ perfusion. The circulatory shock caused by low BP is a situation of mismatch between oxygen delivery and consumption. If not corrected in time, it will lead to high mortality and disability rates (*22*). Hemorrhagic shock can lead to single-organ or multiple-organ failure, especially for organs with high oxygen demand (*10*). Potential brain hypoxia damage caused by reduced cerebral perfusion leads to consciousness disorders and long-term neurological damage after shock (*23*). Our results suggest that cervical LIPUS stimulation can improve cerebral cortical blood flow perfusion aftershock, indicating that stimulation not only increases BP but also increases blood flow to vital organs, providing a promising strategy for antishock. Since LIPUS is portable and economical, the results of our study make noninvasive neuromodulation therapy for shock possible.

Because LIPUS has strong and multiple physical and biological properties, many studies have tried to use ultrasound stimulation to regulate BP. A study found that after the left VN of the hypertensive rabbit model was invasively stimulated with low-intensity focused ultrasound, the rabbit's BP and HR dropped (*24*). Similarly, the team lowered the BP, HR, respiratory rate, and LF/HF ratio in rats with hypertension by using ultrasound to stimulate the isolated left VN, indicating that the parasympathetic nervous system was activated (*25*). In hypertensive animal models, isolating the VN for ultrasound-targeted stimulation has been shown to lower BP, consistent with the function of the VN. Conversely, our noninvasive cervical LIPUS stimulation can increase BP, and the results may be associated with targeted SN excitation. Both of the above-reported studies have creatively separated the VN and stimulated it, while Cao *et al.* used noninvasive transcranial LIPUS to stimulate the solitary nucleus of hypertensive rats, which reduced rat BP. At the same time, the neuronal activity of the solitary nucleus, the ventrolateral periaqueductal gray (vlPAG) in the midbrain, and the tail lateral area of the caudal ventrolateral medulla (CVLM) were also enhanced, but ultrasound stimulation did not cause brain tissue damage (*26*). Thus, the effectiveness of ultrasound stimulation is determined by its target. Our BOLD-fMRI studies revealed that cervical LIPUS stimulation enhances the activity of hypothalamic nuclei involved in BP regulation, such as the OVLT and the SFO. In contrast, transection of the

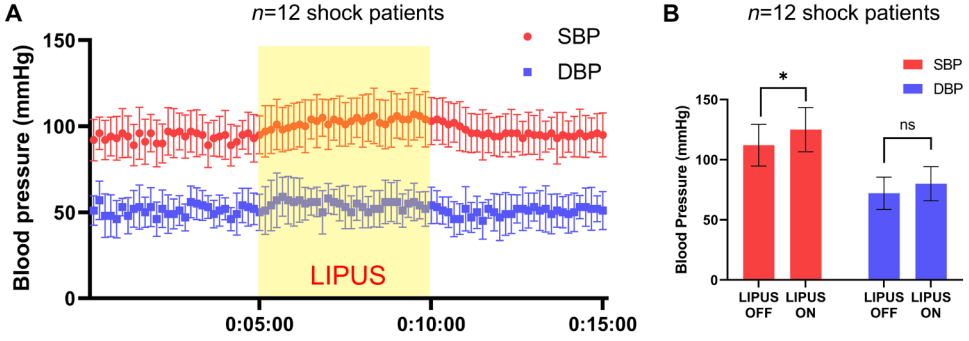

Fig. 7. Small-scale self-control before-after clinical trial showed that cervical LIPUS stimulation elevated BP in shock patients. (**A**) BP in patients before and after LIPUS stimulation ($n = 12$ patients; prestimulation: 0 to 5 min, during stimulation: 5 to 10 min, poststimulation: 10 to 15 min). (**B**) Change in systolic and diastolic BPs of shock patients pre- and post-LIPUS stimulation ($n = 12$ patients; $^*P < 0.05$). SBP: systolic blood pressure; DBP: diastolic blood pressure.

cervical sympathetic trunk only partially attenuated the BP-raising effect of LIPUS, whereas more comprehensive suppression of sympathetic neural activity or ablation of BP-regulatory nuclei completely abolished the BP response elicited by LIPUS. These results further explain the mechanism by which cervical LIPUS stimulation increases BP. Additionally, the carotid sinus and carotid body are important receptors for BP regulation, and these two receptors are under the control of the carotid sinus nerve (*27*). There is evidence that after ultrasound stimulation of the carotid sinus nerve, BP markedly increased (*24*), similar to our results. The carotid sinus nerve is a branch of the glossopharyngeal nerve, and the glossopharyngeal nerve can rapidly modulate sympathetic and parasympathetic nervous activity, which is crucial for regulating BP and HR (*28*). This suggests a correlation between cervical LIPUS stimulation and excitation of the glossopharyngeal nerve. The reason why noninvasive cervical LIPUS in our study raises BP instead of lowering BP may be that the target nerve is the carotid sinus nerve or SN. After the cervical sympathetic trunk was severed, the effect of LIPUS on BP increase was reduced; after further extensive inhibition of sympathetic nervous system activity, LIPUS completely lost its effect of raising BP. At the same time, the HRV analysis results show that LFP and LF/HF ratio increased after stimulation, both of which imply that the stimulation may increase SN excitability to play an anti-shock effect (*29*).

LIPUS has been proven to activate mechanoreceptors, integrin protein, on the cell membrane, thereby activating intracellular focal adhesion kinase (FAK) signaling and promoting its phosphorylation (*30*). The phosphorylation of FAK activates mitogen-activated protein kinase (MAPK) and downstream extracellular signal–regulated kinase (ERK), P38, and c-Jun N-terminal kinase (JNK) signals, thereby playing an important role in cell proliferation, survival, and apoptosis (*31*). In addition, LIPUS activates the phosphatidylinositol 3-kinase (PI3K)/Akt/Nrf2 signaling pathway, alleviating alveolar bone absorption caused by periodontitis (*32*). In heart failure mice, LIPUS activated cardiomyocyte endothelial nitric oxide synthase (eNOS)/nitrogen monoxide (NO)/cGMP-PKG pathway and cardiomyocyte Ca^{2+}-handling system (*33*). Our findings indicate that LIPUS elevates BP by augmenting the excitability of the sympathetic nervous system. Prior research has demonstrated that activation of SNs via knockdown of ADGRA1 or tumor necrosis factor–α (TNF-α) administration leads to the activation of the PI3K/Akt and MAPK kinase (MEK)/ERK pathways in the hypothalamus (*34*, *35*). This aligns with the signal transduction pathways stimulated by LIPUS, reinforcing our assertion that LIPUS modulates sympathetic nervous system activity, resulting in increased BP. The results also depict the potential physiological mechanism of LIPUS-enhanced BP through plasma metabolomics. Metabolomics analysis suggests that metabolites related to vascular smooth muscle contraction and renin secretion increase after LIPUS stimulation; meanwhile, cGMP-PKG, cAMP (adenosine 3′,5′-monophosphate), and sphingolipid signaling pathway–related metabolites are also activated, which is consistent with previous research results (*33*).

After shock occurred, we observed that LIPUS stimulation raised BP and plasma catecholamine levels, and catecholamine levels were positively correlated with SN activity in HRV analysis. The SNs are excited, and the postganglionic neurons of the sympathetic nervous system release catecholamines to contract the vascular smooth muscle and increase BP (*36*). Although different types of shock have different treatment plans, vascular vasoactive drugs are one of the key treatment methods. Shock treatment includes the administration of endogenous catecholamines (epinephrine, norepinephrine, and dopamine), as well as isoproterenol, phenylephrine, milrinone, and other drugs, which have become the mainstays of shock treatment for decades (*37*). However, in patients with hypovolemic shock, excessive use of norepinephrine may lead to reduced renal perfusion (*38*, *39*). Our findings demonstrated that LIPUS stimulation improved cerebral and renal perfusion in rats with hemorrhagic shock. This suggests that LIPUS stimulation not only raises BP but also ameliorates organ perfusion.

We were pleasantly surprised to discover that other teams are also advocating for advancements in the traditional shock treatment paradigm. For decades, this paradigm has remained largely unchanged. These teams are exploring innovative and challenging treatment strategies. Narayan's team found that cervical trigeminal nerve stimulation can improve the activity of the sympathetic nervous system in rats with hemorrhagic shock, and increase cerebral blood flow (CBF) perfusion and brain oxygen tension, thereby improving survival (*12*, *40*). Trigeminal nerve stimulation presents clinical translation challenges due to its invasive nature and the necessity for precise anatomical positioning. Conversely, LIPUS not only elevates BP but also ameliorates multi-organ hypoperfusion. We have demonstrated that LIPUS stimulates BP by exciting the sympathetic nervous system, with elevated levels of vasoactive substances in plasma indicating its potential for sustained BP enhancement. What is encouraging is that our early clinical self-control before-after trial has emphasized the possibility of translating these findings into clinical applications, underscoring its reliability, ease of operation, device portability, and potential for clinical application. The trial shows that cervical LIPUS stimulation can effectively increase the BP of patients with a variety of shock types, not limited to the type of hemorrhagic shock in animal models. The BP regulation center is mainly located in the medulla oblongata, and the increase in BP is related to the specific activation of the rostral ventrolateral medulla (RVLM) (*41*). Therefore, we speculate that LIPUS requires a functional BP regulation center, the brainstem, to take effect. In the future, performing larger sample clinical trials in hemorrhagic shock patients is crucial for validating these positive results and optimizing the clinical use of LIPUS.

In conclusion, cervical LIPUS stimulation represents a noninvasive, convenient, and easily controllable technique applicable for resuscitating shock. It may serve as an innovative first-aid tool for trauma patients and potentially alter the existing paradigm of hemorrhagic shock management. On the basis of the principle of neuromodulation through LIPUS stimulation, LIPUS could play a role in the resuscitation management of patients suffering various types of shock. While the parameters and sustained effects of cervical LIPUS stimulation still require refinement and optimization for patient application, its clinical translation appears imminent. However, this clinical trial is limited to adjunctive treatment for shock patients with stable vital signs. To establish LIPUS as an emergency resuscitation treatment for shock, more extensive research and larger-scale clinical trials are needed.

MATERIALS AND METHODS

Study design

We performed cervical carotid triangle area stimulation using noninvasive LIPUS in normal and hemorrhagic shock rats. All animals in

this study were male Sprague-Dawley rats (HFK Bioscience, Beijing) aged 6 to 8 weeks. While monitoring vital signs before and after stimulation, we also monitored CBF in rats by LASCA, and cardiac function and multiorgan perfusion by time-motion mode ultrasound and Doppler-mode ultrasound. Furthermore, the mechanism of BP elevation by LIPUS stimulation was explored through HRV analysis, peripheral blood metabolomics analysis, and fMRI. Cervical sympathectomy, inhibition of sympathetic activity, or nucleotomy of the BP-related nuclei have been used to elucidate the neuromodulatory mechanisms of LIPUS. A small-scale self-control before-after clinical trial was performed to explore the clinical translational potential of LIPUS.

Arterial monitoring and hemorrhagic shock model

Place rats into a chamber containing 5% isoflurane to induce anesthesia. Once animals are completely anesthetized, place their nose in an anesthesia mask and maintain anesthesia with 2.5% isoflurane. Position the rats supinely on a 37°C warming pad and use depilatory cream to remove hair from the cervical and groin areas. On the left side of the sternohyoid muscle, locate the most prominent pulsation of the left carotid artery and mark it for LIPUS stimulation. Disinfect the skin in the groin area, and make an approximately 2-cm incision along the direction of the femoral artery after palpating the femoral artery in the left groin triangle area. Insert an arterial cannula filled with heparinized saline solution (40 U/ml) into the left femoral artery and connect it to a three-way valve. One end of the three-way valve is connected to a pressure transducer for BP monitoring, and the other end is connected to a syringe containing heparin for blood sampling. The pressure signal is connected to the biological signal acquisition and analysis system (BL-420, Taimeng Co. Ltd., Chengdu, China), which records the arterial pressure waveform. The limb leads for recording the electrocardiogram are inserted subcutaneously into the limbs of the rats and connected to the system. Record the baseline BP waveform and electrocardiogram of each rat for 5 min, excluding animals with initial MAP below 60 mmHg. We established a rat model of hemorrhagic shock as previously reported (*12*). For the rats in the shock group or shock + LIPUS group, we slowly extracted blood at a rate of 0.5 ml/min. This process used a syringe containing 0.1 ml of heparin (6000 U/ml). We continued the extraction until the average arterial pressure remained below 40 mmHg for 5 min.

Cervical nerve transection

To confirm the influence of the cervical sympathetic trunk and the VN on BP elevation during LIPUS, we conducted a nerve transection experiment. For the surgery of nerve transection, we opened the left carotid sheath of the rats and identified and isolated the VN next to the carotid artery, and deep in the carotid artery, we identified and isolated the SN trunk. Depending on the animal group, we used ophthalmic scissors to sever the VN or SN trunk. After removing air from the surgical area with 38°C saline solutions, the skin was sealed with biological glue.

All animal studies were conducted in accordance with the Guide for the Care and Use of Laboratory Animals and were approved by the Tianjin Medical University General Hospital Animal Care and Use Committee (IRB2023-DW-82).

Cervical LIPUS stimulation

Using depilatory cream, remove the hair from the rat's cervical area. Locate the most prominent pulsation of the carotid artery on the left side of the sternohyoid muscle and mark it (fig. S6). Apply the ultrasound coupling agent to the marked area on the skin, and then ensure full contact between the ultrasound probe (DJO FRANCE SAS, Mouguerre, France) and the coupling agent before starting the stimulation. The contact surface of the ultrasound probe is a circular shape with a diameter of 1 cm, generating collimated ultrasound (fig. S6). Monitor the animal's BP and baseline electrocardiogram for at least 5 min before starting the LIPUS stimulation, which lasts for 10 min. After the stimulation stops, continue monitoring the BP and electrocardiogram for at least 5 min. In the LIPUS dose-response experience, rats were randomly divided into groups of the Isppa = 1, 2, or 3 W/cm^2, with five rats in each group. Ten rats with qualified BP were randomly assigned to the skin electrical stimulation and thermal stimulation groups, with five rats in each group. Ten rats were randomly assigned to the VN or SN severed groups, with five rats in each group. Rats for HRV analysis and plasma metabolomics analysis were divided into four groups (control group, control + LIPUS group, shock group, and shock + LIPUS group), initially with 10 rats in each group. Because of the losses during the surgery or shock, the sample sizes were as follows: control group, $n = 9$; control + LIPUS group, $n = 9$; shock group, $n = 8$; and shock + LIPUS group, $n = 8$. All animals were monitored for at least 5 min before the stimulation. Subsequently, the LIPUS intervention groups (control + LIPUS group and shock + LIPUS group) underwent 10 min of stimulation, while the nonstimulation groups (control group and shock group) did not activate the ultrasound generator. After 10 minutes of stimulation, we collected 0.5 ml of arterial blood from each group. The blood was placed in a centrifuge tube containing 10 μl of heparin (6000 U/ml). We then centrifuged the tube at 2000 rpm for 10 minutes. This process allowed us to obtain plasma.

LIPUS parameters: In the dose experiment, Isppa is set to 1 to 3 W/cm^2; for the remaining experiments, the parameters used are as follows: 2-cm^2 ultrasound generator, Isppa of 2 W/cm^2, fundamental frequency of 3 MHz, repetition frequency of 100 Hz, duty cycle of 50%, and pulse duration of 1 ms.

Vital sign collection and analysis

The BL-420 biological signal acquisition and analysis system was used to record the BP waveforms and electrocardiograms. Data are collected at a frequency of 1000 Hz and filtered using low-pass filters and a 50-Hz notch filter to remove noise from the original signals. MAP is obtained from the BP waveform, and HR and R-R intervals are derived from the electrocardiogram data. The software of this system is used to analyze the rat's electrocardiac signal, and HRV analysis is performed based on the R-R interval data of the electrocardiogram waveform. Frequency domain analysis is performed using the software, and HRV parameters are calculated and analyzed. The frequency domain analysis parameters for HRV mainly include total power (TP), which represents the frequency band from 0 to 3.0 Hz; LFP, which represents the frequency band from 0.20 to 0.60 Hz; and HFP, which represents the frequency band from 0.60 to 3.0 Hz. LFP and HFP represent the roles of the sympathetic and parasympathetic nervous systems, respectively. The LF/HF ratio can effectively reflect the balance between the autonomic nervous systems (*42*). LF/HF ratio = LFP/HFP.

H&E staining

The paraffin-embedded skin and nerve tissue sections are cleaned with xylene to remove the wax and then passed through a series of

decreasing alcohol concentrations to rehydrate the tissue. The sections are stained with hematoxylin for 5 min following treatment with acid alcohol to remove the excess hematoxylin. Then, the sections are stained with eosin for 1 min. The samples are passed through increasing alcohol concentrations to dehydrate, followed by xylene to clear the sections, and the samples are finally sealed with a coverslip using a mounting medium for viewing under a microscope.

Prussian blue staining

Prussian blue staining was performed with reference to our previous literature (*43*). Briefly, the sections were incubated in a solution containing 5% potassium ferricyanide (Solarbio, China) and 5% hydrochloric acid (in a 1:1 ratio) for 30 min, followed by rinsing in double-distilled water for 10 min. The nuclei were counterstained blue with hematoxylin.

CBF analysis

As previously reported, LASCA was used to monitor CBF. The Pericam PSI system (Perimed AB, Sweden) was used for laser speckle imaging in rats. For this purpose, each mouse was anesthetized with 1.5% tribromoethanol, the skull was shaved, and the skull was exposed and cleaned through a midline skin incision. The red cross point of the indicator laser (660 nm) was placed at the center of the brain with a fixed measurement distance of 10 cm. The PIM software (Perimed AB, version 1.5) was used to collect CBF signals at a wavelength of 785 nm, and blood perfusion images were obtained. CBF is represented in perfusion units (PUs).

Multi-organ ultrasound examination

All rats undergoing ultrasound examination had their hair shaved from the neck, chest, and abdomen after isoflurane anesthesia. The control group underwent dissection of the femoral artery without blood loss and without activating the cervical ultrasound generator. The shock group achieved the criteria for hemorrhagic shock but did not activate the cervical ultrasound generator. The shock + LIPUS group achieved the criteria for hemorrhagic shock and activated the cervical ultrasound generator. The rats were placed on a 38°C heating pad and examined using the Vevo 3100 small animal ultrasound system (FUJIFILM, Canada).

For cardiac function examination, use a phased array transducer (16 MHz) for echocardiographic examination. For the renal artery, position the transducer in the epigastric and paraumbilical region. Measure renal artery PSVs and EDVs. Calculated parameters include the resistive index (RI) [RI = (PSV − EDV)/PSV]. For the hepatic artery, we placed the transducer in the upper right abdomen. After locating the hepatic artery, we measured the PSV and EDV of the hepatic artery.

Plasma metabolome and analysis

Sample (100 μl) was thoroughly mixed with 400 μl of cold methanol acetonitrile (v/v, 1:1) via vortexing, and then the mixture was processed with sonication for 1 hour in ice baths. The mixture was then incubated at −20°C for 1 hour and centrifuged at 4°C for 20 min with a speed of 14,000*g*. The supernatants were then harvested and dried under vacuum liquid chromatography–mass spectrometry (LC-MS) analysis.

The raw MS data were processed using MS-DIAL (version 5) for peak alignment, retention time correction, and peak area extraction. The metabolites were identified by accuracy mass [mass tolerance <10 parts per million (ppm)] and MS/MS data (mass tolerance <0.02 Da), which were matched with Human metabolome database (HMDB), massbank, and other public databases and our self-built metabolite standard library. In the extracted ion features, only the variables having more than 50% of the nonzero measurement values in at least one group were kept.

R (version 4.0.3) and R packages were used for all multivariate data analyses and modeling. Data were mean-centered using Pareto scaling. Models were built on principal components analysis (PCA), OPLS-DA, and PLS-DA. All the models evaluated were tested for overfitting with methods of permutation tests. The descriptive performance of the models was determined by R2X (cumulative) [perfect model: R2X (cum) = 1] and R2Y (cumulative) [perfect model: R2Y (cum) = 1] values, while their prediction performance was measured by Q2 (cumulative) [perfect model: Q2 (cum) = 1] and a permutation test ($n = 200$). The permuted model should not be able to predict classes: R2 and Q2 values at the y-axis intercept must be lower than those of Q2 and the R2 of the nonpermuted model. OPLS-DA allowed the determination of discriminating metabolites using the VIP. The VIP score value indicates the contribution of a variable to the discrimination between all the classes of samples. Mathematically, these scores are calculated for each variable as a weighted sum of squares of PLS weights. The mean VIP value is 1, and usually, VIP values over 1 are considered significant. A high score is in agreement with a strong discriminatory ability and thus constitutes a criterion for the selection of biomarkers.

The discriminating metabolites were obtained using a statistically significant threshold of VIP values obtained from the OPLS-DA model and two-tailed Student's t test (P value) on the normalized raw data at the univariate analysis level. The P value was calculated by one-way analysis of variance (ANOVA) for multiple groups analysis. Metabolites with VIP values greater than 1.0 and P values less than 0.05 were considered to be statistically significant metabolites. Fold change was calculated as the logarithm of the average mass response (area) ratio between two arbitrary classes. On the other side, the identified differential metabolites were used to perform cluster analyses with the R package.

Blood oxygenation level–dependent fMRI

We acquired transverse-sectional BOLD-fMRI and T2WI images of rats using a 9.4-T MRI system (Bruker, USA). We performed the MRI scan immediately after LIPUS stimulation outside the shielded room. Five rats were scanned before and after LIPUS stimulation for paired comparison. BOLD-fMRI was acquired with the following parameters: echo time = 20 ms, repetition time = 1500 ms, repetitions = 240, slices = 28. T2WI was acquired using the following: effective echo time = 33 ms, repetition time = 2500 ms, echo train length = 8, slices = 28. The MRI raw data were processed and analyzed using the DPABI toolbox (*44*, *45*). Functional images were realigned, reoriented, normalized, and smoothed after the first 10 time points were removed. ALFF and fALFF data were extracted based on the preprocessed data. After registering T2WI images to functional images, data were extracted for analysis by delineating ROIs in conjunction with the rat brain atlas.

Arterial spin labeling perfusion MRI

We acquired coronal-sectional ASL-MRI and T2WI images of rats using a 9.4-T MRI system (Bruker, USA). We performed the MRI scan immediately after LIPUS stimulation outside the shielded room.

ASL-MRI was acquired with the following parameters according to the reference: The inversion times used in this study were 30, 100, 200, 300, 500, 700, 1000, 1200, 1500, 2000, 3000, 5000, and 8000 ms. Imaging was performed with a matrix of 128 × 128, a field of view of 40 × 40 mm, and a section thickness of 2 mm. A single section was acquired. For section-selective inversion, an adiabatic frequency-selective inversion pulse with a hyperbolic secant shape was applied, featuring a bandwidth of 5190 Hz and a section thickness of 5 mm. To quantify renal perfusion, an optimized inversion time of 2000 ms was used. Ten pairs of ASL images, acquired using selective and non-selective inversion pulses, were analyzed to enhance the signal-to-noise ratio.

SN inhibition and nucleotomy

Here, we administered intraperitoneal injections of a solution containing 6-OHDA (20 mg/ml) and 0.1% ascorbic acid to rats over three consecutive days to inhibit SN activity. Following this, under anesthesia, we performed LIPUS stimulation (Isppa = 3 W/cm^2) and monitored BP and HR on the fourth day. Additionally, the SFO nucleus was precisely located at the bregma −0.6 mm and 5 mm deep and received an injection of 10 μg of 6-OHDA for nucleotomy. Six days post-injection, a T2WI scan verified the accuracy of the injection site and the extent of nucleus disruption. Subsequent LIPUS (Isppa = 3 W/cm^2) stimulation under anesthesia and concurrent monitoring of BP and HR were performed on the seventh day.

The small-scale self-control before-after clinical trial

The enrolled patients were admitted during March to June 2024 at the General Hospital of Tianjin Medical University. All shock patients were prioritized for emergency resuscitation upon admission.

Inclusion criteria: (i) age >18 years but <80 years; (ii) admission diagnosis of shock (all types), admission systolic BP < 90 mmHg; (iii) underwent arterial catheterization with real-time BP monitoring; (iv) Glasgow coma scale (GCS) score > 8; (v) relatively stable vital signs without immediate need for surgery.

Exclusion criteria: (i) patients in the perioperative period; (ii) pregnant and lactating patients; (iii) patients with carotid artery plaques; (iv) patients with neck wounds.

Cervical LIPUS stimulation was administered in the following manner: The patient is positioned supine, with the head tilted rightward to expose the left cervical region. The most pronounced pulsation of the carotid artery is identified anterior to the upper portion of the sternocleidomastoid muscle on the left side. After marking the pulsation site, the left neck area is cleansed and disinfected. A suitable quantity of ultrasonic coupling agent is then applied to ensure full contact between the 5-cm^2 ultrasound generator and the skin, and the generator is securely positioned. The LIPUS is initiated with parameters set at an ultrasound frequency of 3 MHz, a pulse frequency of 100 Hz, a duty cycle of 50%, and an Isppa of 3 W/cm^2. All participants underwent a 5-min stimulus, with BP measurements recorded for a minimum of 5 min both before and after the stimulus.

To confirm the safety of cervical LIPUS stimulation, we recruited five health-conscious individuals as volunteers to investigate the effects of LIPUS stimulation on healthy volunteers. BP measurements for healthy volunteers were taken noninvasively using an arm-cuff after they had rested for 10 min in a quiet environment, and again immediately following 5-min LIPUS stimulation, as previously described. BP was measured twice consecutively before LIPUS stimulation to obtain an average value and then measured twice after 5 min of LIPUS stimulation before stopping the stimulation.

This study was approved by the Ethics Committee of Tianjin Medical University General Hospital (IRB2023-YX-267-01). Informed consent was obtained from all subjects or their legal representatives after the patient regained consciousness. The clinical study is registered with the Chinese Clinical Trial Registry (ChiCTR2400093480).

Statistical analysis

Statistical analysis was performed using the GraphPad Prism software (version 9.4). Two independent samples were analyzed using a two-tailed *t* test, and a paired *t* test was conducted to assess the significant difference in the changes in MAP and HR when the LIPUS was turned off and on. Datasets are analyzed with one-way or two-way ANOVA followed by post hoc Tukey's test. $P < 0.05$ was considered as statistically significant. All data were presented as mean ± SD.

Supplementary Materials

The PDF file includes:

Figs. S1 to S6
Tables S1 and S2
Legend for data S1
Legend for movie S1

Other Supplementary Material for this manuscript includes the following:

Data S1
Movie S1

REFERENCES AND NOTES

1. D. S. Kauvar, R. Lefering, C. E. Wade, Impact of hemorrhage on trauma outcome: An overview of epidemiology, clinical presentations, and therapeutic considerations. *J. Trauma* **60**, S3–S11 (2006).
2. J. E. Tintinalli, J. S. Stapczynski, O. J. Ma, D. M. Yealy, G. D. Meckler, D. M. Cline, *Tintinalli's Emergency Medicine: A Comprehensive Study Guide, 8e* (McGraw Hill Education, 2016).
3. J. Cannon, J. Morrison, C. Lauer, D. Grabo, T. Polk, L. Blackbourne, J. Dubose, T. Rasmussen, Resuscitative endovascular balloon occlusion of the aorta (REBOA) for hemorrhagic shock. *Mil. Med.* **183**, 55–59 (2018).
4. D. C. Angus, T. van der Poll, Severe sepsis and septic shock. *N. Engl. J. Med.* **369**, 840–851 (2013).
5. C. Vahdatpour, D. Collins, S. Goldberg, Cardiogenic shock. *J. Am. Heart Assoc.* **8**, e011991 (2019).
6. M. D. Samsky, D. A. Morrow, A. G. Proudfoot, J. S. Hochman, H. Thiele, S. V. Rao, Cardiogenic shock after acute myocardial infarction: A review. *JAMA* **326**, 1840–1850 (2021).
7. O. N. Kislitsina, J. D. Rich, J. E. Wilcox, D. T. Pham, A. Churyla, E. B. Vorovich, K. Ghafourian, C. W. Yancy, Shock - classification and pathophysiological principles of therapeutics. *Curr. Cardiol. Rev.* **15**, 102–113 (2019).
8. S. S. Naidu, D. A. Baran, J. C. Jentzer, S. M. Hollenberg, S. van Diepen, M. B. Basir, C. L. Grines, D. B. Diercks, S. Hall, N. K. Kapur, W. Kent, S. V. Rao, M. D. Samsky, H. Thiele, A. G. Truesdell, T. D. Henry, SCAI SHOCK Stage Classification Expert Consensus Update: A Review and Incorporation of Validation Studies: This statement was endorsed by the American College of Cardiology (ACC), American College of Emergency Physicians (ACEP), American Heart Association (AHA), European Society of Cardiology (ESC) Association for Acute Cardiovascular Care (ACVC), International Society for Heart and Lung Transplantation (ISHLT), Society of Critical Care Medicine (SCCM), and Society of Thoracic Surgeons (STS) in December 2021. *J. Am. Coll. Cardiol.* **79**, 933–946 (2022).
9. K. Kashani, T. Omer, A. D. Shaw, The intensivist's perspective of shock, volume management, and hemodynamic monitoring. *Clin. J. Am. Soc. Nephrol.* **17**, 706–716 (2022).
10. A. Fecher, A. Stimpson, L. Ferrigno, T. H. Pohlman, The pathophysiology and management of hemorrhagic shock in the polytrauma patient. *J. Clin. Med.* **10**, 4793 (2021).
11. P. E. Marik, M. Weinmann, Optimizing fluid therapy in shock. *Curr. Opin. Crit. Care* **25**, 246–251 (2019).
12. C. Li, A. Chiluwal, A. Afridi, W. Chaung, K. Powell, W. L. Yang, P. Wang, R. K. Narayan, Trigeminal nerve stimulation: A novel method of resuscitation for hemorrhagic shock. *Crit. Care Med.* **47**, e478–e484 (2019).

13. X. Jiang, O. Savchenko, Y. Li, S. Qi, T. Yang, W. Zhang, J. Chen, A review of low-intensity pulsed ultrasound for therapeutic applications. *IEEE Trans. Biomed. Eng.* **66**, 2704–2718 (2019).
14. W. Legon, T. F. Sato, A. Opitz, J. Mueller, A. Barbour, A. Williams, W. J. Tyler, Transcranial focused ultrasound modulates the activity of primary somatosensory cortex in humans. *Nat. Neurosci.* **17**, 322–329 (2014).
15. S. S. Yoo, A. Bystritsky, J. H. Lee, Y. Zhang, K. Fischer, B. K. Min, N. J. McDannold, A. Pascual-Leone, F. A. Jolesz, Focused ultrasound modulates region-specific brain activity. *Neuroimage* **56**, 1267–1275 (2011).
16. C. Rabut, S. Yoo, R. C. Hurt, Z. Jin, H. Li, H. Guo, B. Ling, M. G. Shapiro, Ultrasound technologies for imaging and modulating neural activity. *Neuron* **108**, 93–110 (2020).
17. R. Martínez-Fernández, J. U. Máñez-Miró, R. Rodríguez-Rojas, M. Del Álamo, B. B. Shah, F. Hernández-Fernández, J. A. Pineda-Pardo, M. Monje, B. Fernández-Rodríguez, S. A. Sperling, D. Mata-Marín, P. Guida, F. Alonso-Frech, I. Obeso, C. Gasca-Salas, L. Vela-Desojo, W. J. Elias, J. A. Obeso, Randomized trial of focused ultrasound subthalamotomy for Parkinson's Disease. *N. Engl. J. Med.* **383**, 2501–2513 (2020).
18. R. Martínez-Fernández, R. Rodríguez-Rojas, M. Del Álamo, F. Hernández-Fernández, J. A. Pineda-Pardo, M. Dileone, F. Alonso-Frech, G. Foffani, I. Obeso, C. Gasca-Salas, E. de Luis-Pastor, L. Vela, J. A. Obeso, Focused ultrasound subthalamotomy in patients with asymmetric Parkinson's disease: A pilot study. *Lancet Neurol.* **17**, 54–63 (2018).
19. G. Leinenga, J. Götz, Scanning ultrasound removes amyloid-β and restores memory in an Alzheimer's disease mouse model. *Sci. Transl. Med.* **7**, 278ra33 (2015).
20. D. Folloni, L. Verhagen, R. B. Mars, E. Fouragnan, C. Constans, J. F. Aubry, M. Rushworth, J. Sallet, Manipulation of subcortical and deep cortical activity in the primate brain using transcranial focused ultrasound stimulation. *Neuron* **101**, 1109–1116.e5 (2019).
21. L. Verhagen, C. Gallea, D. Folloni, C. Constans, D. E. Jensen, H. Ahnine, L. Roumazeilles, M. Santin, B. Ahmed, S. Lehericy, M. C. Klein-Flügge, K. Krug, R. B. Mars, M. F. Rushworth, P. Pouget, J. F. Aubry, J. Sallet, Offline impact of transcranial focused ultrasound on cortical activation in primates. *eLife* **8**, e40541 (2019).
22. S. D. Hutchings, D. N. Naumann, P. Hopkins, C. Mellis, P. Riozzi, S. Sartini, J. Mamuza, T. Harris, M. J. Midwinter, J. Wendon, Microcirculatory impairment is associated with multiple organ dysfunction following traumatic hemorrhagic shock: The MICROSHOCK study. *Crit. Care Med.* **46**, e889–e896 (2018).
23. K. K. Ida, D. A. Otsuki, A. T. C. Sasaki, E. S. Borges, L. U. C. Castro, T. R. Sanches, M.-H. M. Shimizu, L. C. Andrade, J.-O. C. Auler Jr., A. Dyson, K. J. Smith, J. A. R. Filho, L.-M. Sá Malbouisson, Effects of terlipressin as early treatment for protection of brain in a model of haemorrhagic shock. *Crit. Care* **19**, 107 (2015).
24. N. Ji, W. H. Lin, F. Chen, L. Xu, J. Huang, G. Li, Blood pressure modulation with low-intensity focused ultrasound stimulation to the vagus nerve: A pilot animal study. *Front. Neurosci.* **14**, 586424 (2020).
25. N. Ji, Y. Li, J. Wei, F. Chen, L. Xu, G. Li, W. H. Lin, Autonomic modulation by low-intensity focused ultrasound stimulation of the vagus nerve. *J. Neural Eng.* **19**, 066036 (2022).
26. F. Cao, J. Zhang, D. Li, M. Wang, C. Lai, T. Xu, A. Bouakaz, P. Ren, M. Wan, J. Han, S. Zhang, Non-invasive ultrasound modulation of solitary tract nucleus exerts a sustainable antihypertensive effect in spontaneously hypertensive rats. *IEEE Trans. Biomed. Eng.* **70**, 1869–1878 (2023).
27. C. G. Goetz, *Textbook of Clinical Neurology* (Elsevier Health Sciences, 2007).
28. L. Norcliffe-Kaufmann, The vagus and glossopharyngeal nerves in two autonomic disorders. *J. Clin. Neurophysiol.* **36**, 443–451 (2019).
29. J. Kubanek, P. Shukla, A. Das, S. A. Baccus, M. B. Goodman, Ultrasound elicits behavioral responses through mechanical effects on neurons and ion channels in a simple nervous system. *J. Neurosci.* **38**, 3081–3091 (2018).
30. T. Kokubu, N. Matsui, H. Fujioka, M. Tsunoda, K. Mizuno, Low intensity pulsed ultrasound exposure increases prostaglandin E2 production via the induction of cyclooxygenase-2 mRNA in mouse osteoblasts. *Biochem. Biophys. Res. Commun.* **256**, 284–287 (1999).
31. E. Tanaka, S. Kuroda, S. Horiuchi, A. Tabata, T. El-Bialy, Low-intensity pulsed ultrasound in dentofacial tissue engineering. *Ann. Biomed. Eng.* **43**, 871–886 (2015).
32. S. Ying, M. Tan, G. Feng, Y. Kuang, D. Chen, J. Li, J. Song, Low-intensity pulsed ultrasound regulates alveolar bone homeostasis in experimental periodontitis by diminishing oxidative stress. *Theranostics* **10**, 9789–9807 (2020).
33. Y. Monma, T. Shindo, K. Eguchi, R. Kurosawa, Y. Kagaya, Y. Ikumi, S. Ichijo, T. Nakata, S. Miyata, A. Matsumoto, H. Sato, M. Miura, H. Kanai, H. Shimokawa, Low-intensity pulsed ultrasound ameliorates cardiac diastolic dysfunction in mice: A possible novel therapy for heart failure with preserved left ventricular ejection fraction. *Cardiovasc. Res.* **117**, 1325–1338 (2021).
34. X. H. Zhang, L. Y. Tang, X. Y. Wang, C. L. Shen, W. F. Xiong, Y. Shen, Y. H. Wan, Y. B. Wu, Y. C. Wang, H. X. Zhang, S. Y. Lu, J. Fei, Z. G. Wang, ADGRA1 negatively regulates energy expenditure and thermogenesis through both sympathetic nervous system and hypothalamus-pituitary-thyroid axis in male mice. *Cell Death Dis.* **12**, 362 (2021).
35. S. G. Wei, Y. Yu, R. B. Felder, TNF-α-induced sympathetic excitation requires EGFR and ERK1/2 signaling in cardiovascular regulatory regions of the forebrain. *Am. J. Physiol. Heart Circ. Physiol.* **320**, H772–H786 (2021).
36. A. B. Dahlstroem, B. E. Zetterstroem, Noradrenaline stores in nerve terminals of the spleen: Changes during hemorrhagic shock. *Science* **147**, 1583–1585 (1965).
37. D. Annane, L. Ouanes-Besbes, D. de Backer, D. U. Bin, A. C. Gordon, G. Hernández, K. M. Olsen, T. M. Osborn, S. Peake, J. A. Russell, S. Z. Cavazzoni, A global perspective on vasoactive agents in shock. *Intensive Care Med.* **44**, 833–846 (2018).
38. K. Hoogenberg, A. J. Smit, A. R. Girbes, Effects of low-dose dopamine on renal and systemic hemodynamics during incremental norepinephrine infusion in healthy volunteers. *Crit. Care Med.* **26**, 260–265 (1998).
39. M. Richer, S. Robert, M. Lebel, Renal hemodynamics during norepinephrine and low-dose dopamine infusions in man. *Crit. Care Med.* **24**, 1150–1156 (1996).
40. M. B. Mulder, K. G. Proctor, A new pathway to treat hemorrhagic shock. *Crit. Care Med.* **47**, 882–883 (2019).
41. E. Colombari, M. A. Sato, S. L. Cravo, C. T. Bergamaschi, R. R. Campos Jr., O. U. Lopes, Role of the medulla oblongata in hypertension. *Hypertension* **38**, 549–554 (2001).
42. B. Xhyheri, O. Manfrini, M. Mazzolini, C. Pizzi, R. Bugiardini, Heart rate variability today. *Prog. Cardiovasc. Dis.* **55**, 321–331 (2012).
43. C. Wu, M. Du, R. Yu, Y. Cheng, B. Wu, J. Fu, W. Tan, Q. Zhou, E. Balawi, Z. B. Liao, A novel mechanism linking ferroptosis and endoplasmic reticulum stress via the circPtpn14/miR-351-5p/5-LOX signaling in melatonin-mediated treatment of traumatic brain injury. *Free Radic. Biol. Med.* **178**, 271–294 (2022).
44. C. G. Yan, M. Rincón-Cortés, C. Raineki, E. Sarro, S. Colcombe, D. N. Guilfoyle, Z. Yang, S. Gerum, B. B. Biswal, M. P. Milham, R. M. Sullivan, F. X. Castellanos, Aberrant development of intrinsic brain activity in a rat model of caregiver maltreatment of offspring. *Transl. Psychiatry* **7**, e1005 (2017).
45. C. G. Yan, X. D. Wang, X. N. Zuo, Y. F. Zang, DPABI: Data processing & analysis for (resting-state) brain imaging. *Neuroinformatics* **14**, 339–351 (2016).

Acknowledgments: We would like to thank K. Xie from the ICU of Tianjin Medical University General Hospital and L. Wang from the Emergency Department for their assistance with the clinical trial of this study. We would like to thank Y. He from the Department of Radiology at Tianjin Medical University General Hospital for her assistance with the MRI scanning. We thank Shanghai Bioprofile Technology Co. Ltd. for the technical help. We would like to thank BioRender.com for providing the materials that helped us complete the diagram (Figure 1). **Funding:** This work was supported by the National Natural Science Foundation of China (grant 82471497 to X.W., S.Z., and R.J.; grant 82071390 to R.J.; grant 82271394 to R.J.; grant 82101434 to R.J.; grant 82001323 to C.G.). **Author contributions:** Conceptualization: C.W., Y.T., T.L., S.A., Y.Q., W.J., X.W., S.Z., and R.J. Methodology: C.W., Y.T., T.L., S.A., C.G., J.Y., W.J., Z.S., X.W., and S.Z. Software: C.W., T.L., M.N., Z.S., X.W., and S.Z. Validation: C.W., Y.T., T.L., Y.Q., X.W., and S.Z. Formal analysis: C.W., T.L., W.J., X.W., and S.Z. Investigation: Y.T., C.G., M.N., W.J., C.L., X.W., S.Z., and R.J. Resources: S.A., C.G., J.Y., W.J., C.L., X.W., S.Z., and R.J. Data curation: Y.T., C.G., M.N., W.J., X.W., S.Z., and R.J. Writing—original draft: C.W., T.L., W.J., X.W., and S.Z. Writing—review and editing: C.W., Y.T., T.L., S.A., Y.Q., J.Y., M.L., M.N., W.J., Z.S., C.L., Q.L., X.W., S.Z., and R.J. Visualization: C.W., Y.T., T.L., M.N., W.J., X.W., and S.Z. Supervision: M.L., Q.L., X.W., S.Z., and R.J. Funding acquisition: C.G., X.W., S.Z., and R.J. Project administration: C.G., X.W., S.Z., and R.J. **Competing interests:** C.W., Y.T., and R.J. have applied for a Chinese invention patent (2024103394013) on 23 March 2024. The authors declare that they have no competing interests. **Data and materials availability:** All data needed to evaluate the conclusions in the paper are present in the paper and/or the Supplementary Materials.

Submitted 24 August 2024
Accepted 11 February 2025
Published 19 March 2025
10.1126/sciadv.ads6947